Nuclear Instruments and Methods in Physics Research A 662 (2012) 26–32

Contents lists available at SciVerse ScienceDirect

Nuclear Instruments and Methods in Physics Research A

journal homepage: www.elsevier.com/locate/nima

A prototype TOF PET detector module using a micro-channel plate photomultiplier tube with waveform sampling

H. Kim [a,*], C.-T. Chen [a], H. Frisch [b], F. Tang [b], C.-M. Kao [a]

[a] Department of Radiology, University of Chicago, Chicago, IL 60637, United States
[b] Enrico Fermi Institute, University of Chicago, Chicago, IL 60637, United States

ARTICLE INFO

Article history:
Received 15 July 2011
Received in revised form
30 August 2011
Accepted 29 September 2011
Available online 8 October 2011

Keywords:
Positron emission tomography
Micro-channel plate photomultiplier
Transmission-line readout
Waveform sampling
Time resolution

ABSTRACT

We are exploring a large area flat panel micro-channel plate photomultiplier tube (MCP PMT) under development for an application to Time-of-Flight Positron Emission Tomography (TOF PET). High speed waveform sampling with transmission-lines is adopted for reading out the signal with precise time and space information with a small number of low-power channels. As a demonstration of the concept, detector modules have been built using 2 in. × 2 in. Photonis Planacon MCP PMTs (XP85022) and prototype transmission-line (TL) boards. The signals from the MCP PMT through the transmission-lines are sampled by DRS4 evaluation boards running at 5 giga-samples per second (GS/s). The event information is extracted by processing the digitized waveforms. For experimental tests, a single $3 \times 3 \times 10$ mm^3 LYSO crystal is optically coupled to each MCP PMT; the detector responses to 511 keV annihilation photon from a ^{22}Na source are measured using the data taken in coincidence mode. As a preliminary result, we obtain a position resolution of ~2.8 mm (0.3 mm) (FWHM) along (perpendicular to) the transmission-line, ~309 ps (FWHM) for coincidence time resolution, and ~14% (FWHM) of energy resolution at 511 keV. This initial result gives a promise that the large area MCP PMT is applicable to TOF PET.

© 2011 Elsevier B.V. All rights reserved.

1. Introduction

Micro-channel plate photomultiplier tube [1] (MCP PMT) features fast timing [2,3] and high gain, which make it a promising photodetector for Time-of-Flight Positron Emission Tomography (TOF PET). Relatively small thickness and low sensitiveness to magnetic field [4,5] are also advantageous in integrating with other imaging modality (e.g., MRI). Due to recent development efforts [6], a large area (8 in. × 8 in.) MCP PMT would be available in the near future at economical cost. Previously we have investigated a PET detector design [7] employing a large area MCP PMT and a transmission-line readout scheme by using GEANT4 simulation. The simulation results show that the large area flat-panel MCP PMT is applicable to PET instrumentation to provide fast coincidence timing resolution, good energy and spatial resolution. In this design, data acquisition (DAQ) is achieved by using high speed waveform sampling of the MCP PMT anode signals through transmission-line strips. Conventional data acquisition for PET has relied on two electronics chains to obtain energy and time information separately. In the waveform sampling-based DAQ, event information is extracted in an unified way by processing the digitized waveform. The digitized waveform allows to use advanced digital processing algorithms which can be easily implemented and upgraded in field-programmable gate arrays (FPGA) without any changes in the front-end electronics, for instance, to improve the coincidence time. As fast sampling technology (1–20 GS/s) [8–12] is advancing rapidly and becoming available at low cost, interests in using waveform sampling in PET is increasing [13,14].

We have developed prototype detector modules employing MCP PMTs, transmission-line strips and waveform sampling to demonstrate the detector design concept conceived in the simulation study. The detector module is built using a Photonis XP85022 MCP PMT [15] and a prototype transmission-line board. For data acquisition, DRS4 [10] boards are used to digitize the waveforms from the MCP PMT/TL and tested as a possible candidate for the future front-end electronics development. As a first step to assess the performance of the module, each MCP PMT/TL module is coupled with a single $3 \times 3 \times 10$ mm^3 LYSO crystal, and experimental tests are conducted to measure the response to 511 keV annihilation photon.

The rest of the paper is organized as follows. In Section 2, the detector module and experimental setup to measure the performance of the prototype detector modules, and signal processing to derive the event information are described. The results obtained from the experimental tests are reported in Section 3. Discussions and summary of the study are given in Section 4.

* Corresponding author. Tel.: +1 773 702 0043.
E-mail address: heejongkim@uchicago.edu (H. Kim).

0168-9002/$ - see front matter © 2011 Elsevier B.V. All rights reserved.
doi:10.1016/j.nima.2011.09.059

2. Materials and methods

2.1. A prototype module

We have built two detector modules using custom-made Photonis XP85022 (2 in. × 2 in.) MCP PMTs and prototype TL boards [16]. The XP85022 is a chevron MCP PMT with a pore diameter of 25 μm, and has 1024 (32 × 32) anode grid with a 1.6 mm pitch between adjacent anodes. The transmission-line board has 32 anode strips with a 1.6 mm pitch, and each strip is coupled to 32 anodes on a row of the XP85022. Anode structure of the XP85022 and a bare transmission board before assembly is shown in Fig. 1(a). The transmission-line board used in the previous study equipped only four connectors for reading out four central strips. For this study, newly built transmission-line boards are used to make all 32 strips on the board readable. Fig. 1(b) shows a XP85022 mounted on the transmission-line board. On the left-hand side of the board, the strip-lines are terminated with 50 Ω resistor, except for the central four channels that are used for time difference measurement at both ends of a strip-line. The signals from the strip-lines are readout by use of DRS4 evaluation boards [17] developed at PSI, Switzerland. Domino Ring Sampler (DRS) is a high speed waveform sampling chip based on switched capacitor array technology. A DRS4 evaluation board provides four input channels, each with 1024 capacitor cells. Sampling frequency of the DRS4 chip is adjustable between 0.7 and 5 GS/s. In our test, the sampling frequency of the board is set to 5 GS/s, which provides enough samples on the rising part of the pulse for precise time decision. Approximately 200 ns of overall sampling time (1024/5 GS/s) allows to fully record the LYSO scintillator signal. The board is controlled through a USB interface, and the inside of the board is shown in Fig. 1(c).

2.2. Experimental setup

In this study, a single LYSO crystal is used to stop 511 keV annihilation photons and simplify the experimental setup. An LYSO crystal with the dimension of $3 \times 3 \times 10\ mm^3$ (Proteus Inc.) is optically coupled, using optical gel (refractive index=1.46) from Cargille Labs., to the MCP PMT window via a $3 \times 10\ mm^2$ side, and all the other sides of the crystal were wrapped using white Teflon. The 10 mm-length axis of the crystal is aligned parallel to the strip-line direction on the middle of the MCP PMT. Two MCP PMT/TL modules with LYSO crystal are placed 5 cm apart from each other as shown in Fig. 2, and a ^{22}Na source with a 0.25 mm active diameter is placed at the middle of the two modules. The high voltage of the XP85022 is set to −2150 V at which the gain of the MCP PMT is about 10^6. The signals from the transmission-line are amplified by use of LeCroy 612A fast amplifiers (10× gain) to match with the input dynamic range of the DRS4 board (from −500 to +500 mV) and enhance signal-to-noise ratio (SNR). The gain in the SNR, a factor of ∼2, by introducing the amplifier is estimated by noting the ratio between the noise level of the DRS4 board (∼0.4 mV RMS, see Section 3.1 below) and the amplifier (∼2 mV RMS). Therefore, while the signal is amplified 10 times, the noise is amplified ∼5 times only. The final waveforms are recorded by use of three DRS4 evaluation boards running at 5 GS/s with external triggers. To prepare trigger signals to these boards, the LeCroy 428F Fan In/Out modules are used to sum-up the four highest strip-line signals, and the summed outputs are fed to the LeCroy 623B discriminators operating at a 100 mV threshold. Coincidence decision is made by using an LeCroy 622 with logic outputs from the discriminators. Due to the limited number of channels of the readout electronics (12 channels in total), only six strip-lines having the highest amplitudes are readout for each MCP PMT/TL module. A block diagram illustrating the measurement setup is shown in Fig. 2. For some measurements, one of the MCP PMT/TL modules is replaced by a R9800 Hamamatsu PMT to allow more readout channels to the other MCP PMT/TL module.

2.3. Signal processing

One coincidence event consists of 12 waveforms, each waveform having 1024 sampling points with ∼200 ps sampling interval for a ∼200 ns duration. An example waveform is shown in Fig. 3. The trigger delay in the board is adjusted to have the pulse start from ∼30 ns on the time axis. The signal-processing steps to obtain event information from the digitized waveforms are summarized below.

- The base-line of the waveform is corrected by using the first 20 ns data for each waveform. Though the amplitude offset of DRS4 is negligible, the base-line correction is carried out to have consistent reference amplitude before applying time pick-up methods.
- The energy of a strip-line is estimated by summing-up all the base-line corrected samples for 150 ns from the pulse start. The energy of an MCP PMT/TL module is obtained by summing all energies obtained for its constituent strip-lines.
- Since time information is in the rising part of pulse, the waveform in [20–40] ns region is selected for time processing.
- A low-pass filter is first applied to this sub-waveform to reduce high-frequency noise. Then, a cubic-spline interpolation [18] is applied to up-sample this filtered sub-waveform having a 200 ps sampling interval to a new waveform having a finer 10 ps sampling interval.
- Time pick-up methods are applied on the rising part of the interpolated waveform. The leading-edge discriminator (d-LED) and constant fraction discriminator (d-CFD) are implemented and used to obtain the coincidence time between two MCP PMT/TL modules. Give a threshold amplitude, d-LED calculates the time crossing the threshold by linear interpolation using two points adjacent the threshold. In d-CFD method, the threshold is set to a fraction of the maximum amplitude of the waveform.
- For time difference measurement at the two ends of a strip-line, multiple leading edge discriminator (m-LED) is applied. Since the

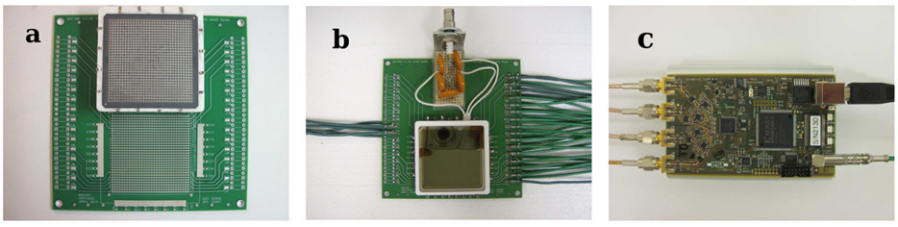

Fig. 1. (a) A Photonis XP85022 MCP PMT and a transmission-line board before assembly. Structure of the transmission-line board and anodes of the XP85022 on the back are shown. The transmission-line board contains 32 strip-lines running horizontally, each providing 32 contact points. The spacing of the strip-lines and their contact points match exactly to that of the 32 × 32 anode structure of the MCP PMT. (b) A prototype module after assembly. The 32 strip-lines of the board can be connected to DRS4 inputs through LEMO cables on the right-hand side. The other ends of the strip-lines are terminated using 50 Ω, except for the central four channels. (c) A DRS4 evaluation board provides four input channels for waveform sampling, an external trigger, and a USB interface.

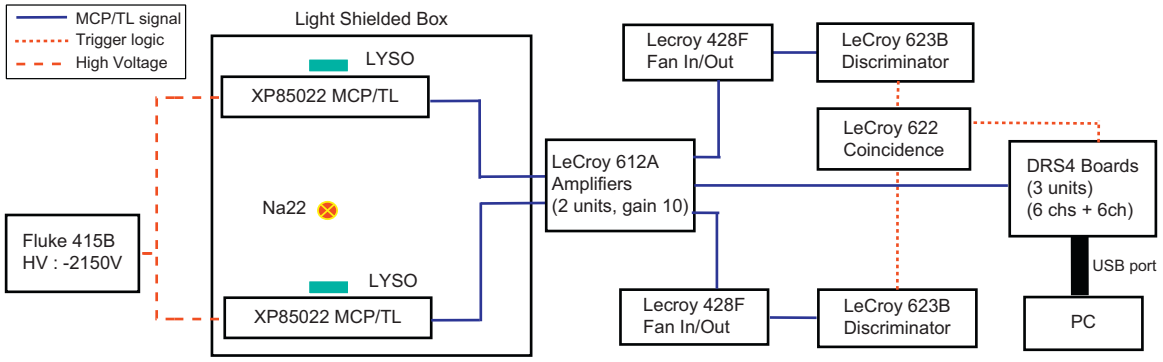

Fig. 2. A block diagram of the experimental setup with two modules in coincidence mode. For some measurements, one of the MCP PMT/TL modules is replaced by a Hamamatsu R9800 PMT.

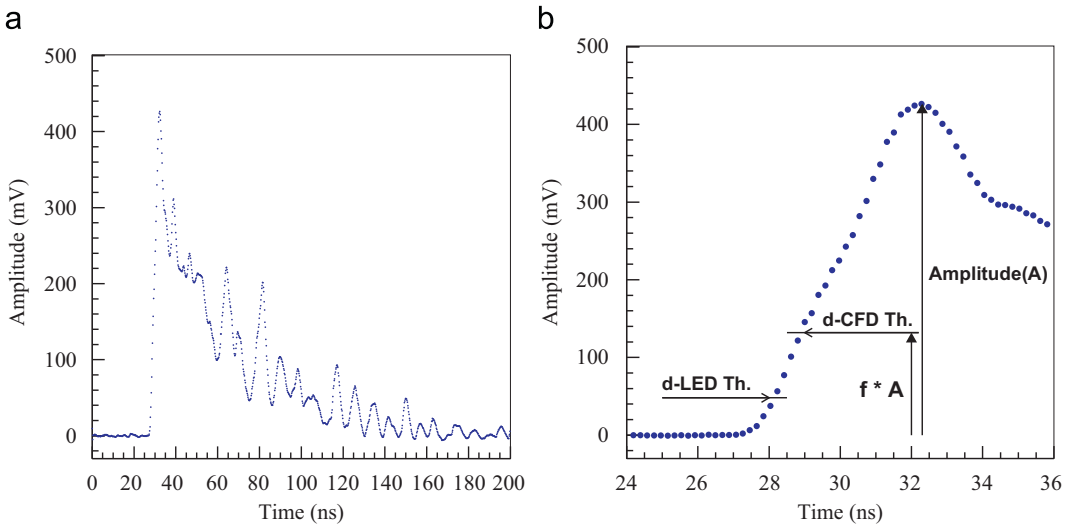

Fig. 3. (a) A waveform from a strip-line recorded by the DRS4. (b) Close-up of the rising part of the same waveform. The time pick-up in the leading-edge discriminator (d-LED) uses a fixed threshold, while the constant fraction discriminator (d-CFD) relies on the varied threshold with the pulse amplitude (A) and the fraction (f) coefficient. The polarity of the waveform is flipped for display purpose.

two waveforms on the two ends of a strip-line are identical in amplitude and shape, time determined from multiple thresholds on the rising part of the pulse can be more accurate than d-LED or d-CFD that uses a single reference point. Approximately 10 thresholds between 10% and 80% of the maximum amplitude are used in the m-LED method. The threshold points are selected to have $\sim$200 ps intervals between adjacent ones.

- The crystal position perpendicular to the strip-lines direction is determined from the strips' coordinates weighted by their energies. The position along the strip-line is obtained from the time difference measured at the two ends of the strip-line.

In this study, all the recorded waveform are saved into a hard disk for off-line analysis. For larger scale systems, transferring/saving the entire waveform to the disk can be problematic. Therefore, the methods described above are relatively simple so that they can be easily implemented in the FPGA firmware for on-line processing. More sophisticated methods will be explored in our future studies.

3. Results

3.1. Characteristics of the DRS4 board

The performance properties of the DRS4 chip are well described in its specification data sheet [17]. Some of the DRS4 characteristics, especially important for precise time determination, are measured; these include the noise level and the electronic time resolution. The DRS4 evaluation board is equipped with on-board utilities for amplitude and time calibration. In this study, we rely on these embedded utilities for calibration. To measure the noise level of the DRS4 board, all the inputs of the board are disconnected, and waveforms data are acquired using an external trigger initiated by a pulse generator (LeCroy 9211). From the amplitude distribution of the 1024 sampled points, shown in Fig. 4(a), the noise level is found to be $\sim$0.4 mV RMS. We also repeat this measurement 5000 times, and Fig. 4(b) shows the histogram of the resulting 5000 RMS values, showing a noise level of 0.40 ± 0.02 mV RMS. The observed noise level is consistent with the value (0.35 mV RMS) in the specification.

The electronic time resolution of the DRS4 board is measured from the differential time of two of its input channels. For this measurement, a 2 ns width pulse (FWHM) is generated using a pulse generator (LeCroy 9211), and is split into two identical pulses by using a T connector. The two pulses after the T connector are fed to two input channels of the DRS4 board. The resulting waveforms are processed following the procedures described in Section 2.3. Since the two pulses are identical, the m-LED method is used for time pick-up. Fig. 5 shows the resulting differential time with $\sim$430 mV input amplitude. From the distribution, the time resolution is measured to be $\sim$7.0 ps FWHM (4.9 ps FWHM for single channel). Due to its dependence on signal-to-noise ratio, the electronic time resolution becomes

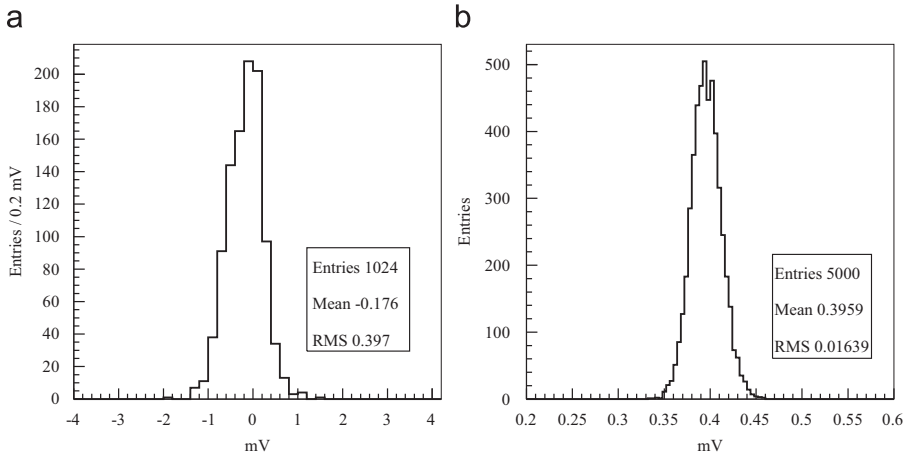

Fig. 4. (a) DRS4 noise level (~ 0.4 mV RMS) of 1024 capacitor cells in a single measurement. (b) Histogram of the RMS of the noise level measured individually from 5000 measurements.

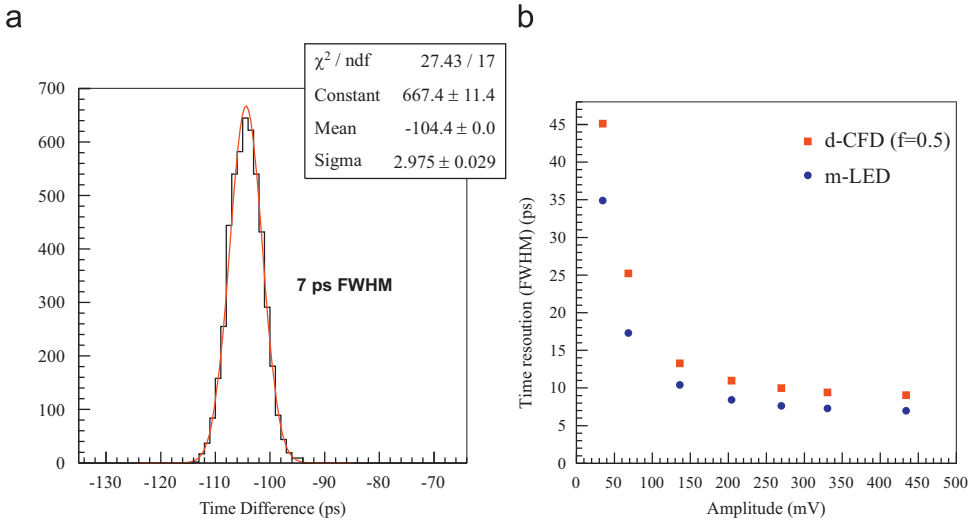

Fig. 5. (a) Differential time between two identical waveforms recorded in two DRS4 channels gives the electronic time resolution, ~ 7 ps at 430 mV input amplitude. (b) Time resolution using the m-LED is shown as a function of the input signal amplitude to the DRS4, and results with the d-CFD is also shown for comparison.

larger with lower amplitude input. Time resolution measured by varying the input amplitude to DRS4 board is shown in Fig. 5.

3.2. Energy to 511 keV photon

The energy spectrum measured by a MCP PMT/TL module to 511 keV photon is shown in Fig. 6(a). The energy is obtained by integrating the waveforms from 10 strip-lines having the highest energy. The integration time is set to 150 ns from the time the pulse starts. This integration time is sufficient to cover the full length of the LYSO signal (~ 40 ns decay time constant). From the pulse-height spectrum, the energy resolution at 511 keV is measured to be ~ 14% (FWHM). For this energy measurement, one of MCP PMT/TL modules in the test setup (Fig. 2) is replaced by a Hamamatsu R9800 PMT coupled with a LSO crystal ($6.3 \times 6.3 \times 25$ mm^3). In this way, 10 input channels of the DRS4 boards are allocated to a MCP PMT/TL module to collect MCP PMT signals spread across several strip-lines. To find an optimal integration time, the energy resolution is also measured by reducing the integration time down to 20 ns and the result is shown in Fig. 6(b), in which 23% at 0 ns represents the energy resolution by using the maximum amplitude of the summed waveform. As shown, the energy resolution is not improved much with increased integration time beyond 50 ns. The DRS4 chip supports partial waveform sampling, called region-of-interest readout, which uses only a subset of the 1024 capacitor cells. The observation made in Fig. 6 can be considered for customizing the readout electronics to, for example, to increase the acquisition rate and reduce pile up.

3.3. Coincidence time

The coincidence time between the two MCP PMT/TL modules is measured for events in the photo-peak; the energy of each MCP PMT/TL module is obtained by summing-up energies from six strip-lines, and events with [400,650] keV energy for both modules are selected. To determine the event time for each strip-line, the d-LED and d-CFD threshold are applied on the rising part of the waveform. Fig. 7(a) shows the differential time of two detector modules. From Gaussian fit on the distribution, the coincidence time resolution is measured to be ~ 309 ps (FWHM). The result shown in the figure is obtained by applying the d-LED method with 4 mV threshold for six constituent strip waveforms for each module; the average of six strips is taken as the event

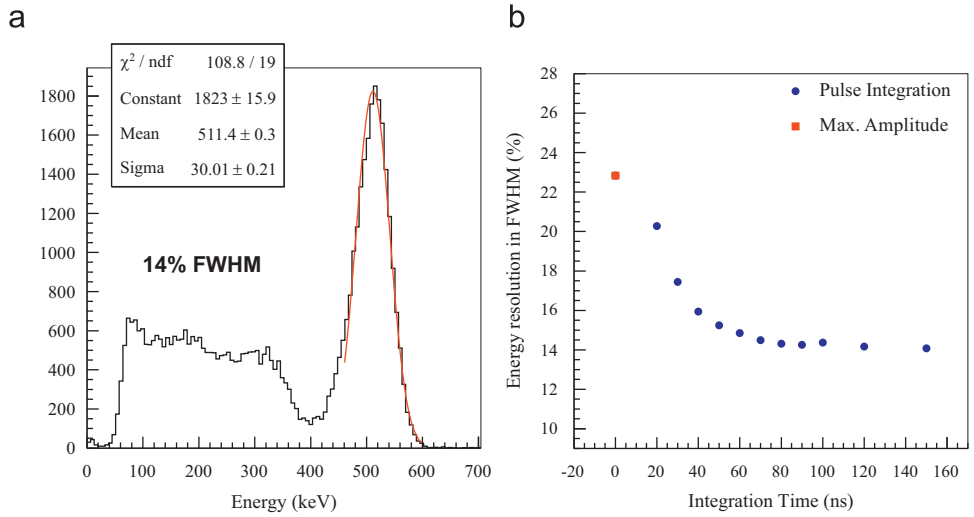

Fig. 6. (a) Pulse-height spectrum obtained by a MCP PMT/TL module and a ^{22}Na source. Ten strip-line signals are summed-up and the peak is normalized to 511 keV. (b) Energy resolution as a function of pulse integration time for energy calculation.

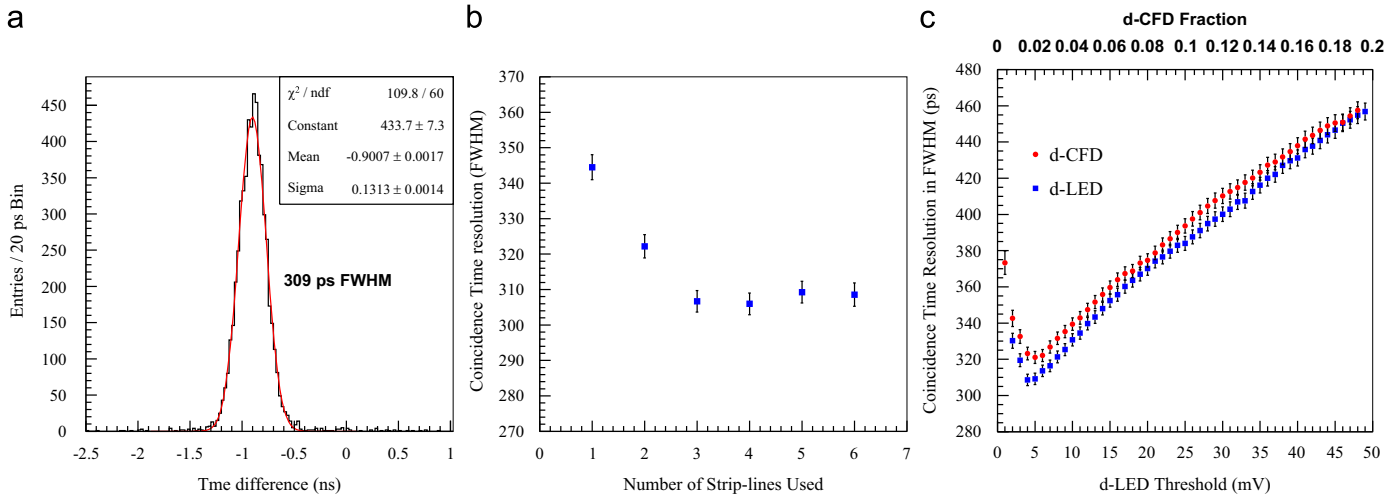

Fig. 7. (a) Differential time between two MCP PMT/TL modules in 511 keV photo-peak events. Approximately 309 ps FWHM of coincidence time resolution is obtained by applying the d-LED with 4 mV threshold. (b) Coincidence time resolution vs. the number of strip-lines used for time decision. (c) Coincidence time resolution dependence on the applied threshold in d-LED and on the fraction in d-CFD.

time. Fig. 7(b) shows the coincidence time resolution as a function of the number of highest-energy strip-line used in the event time determination. Due to signal spread and the fine pitch of the strip-line, the time determined using three or four strip-lines gives better result than using a single strip-line with the highest energy. The time resolution dependence on the threshold level of d-LED is shown in Fig. 7(c), along with the d-CFD results. The low noise level of DRS4 and MCP PMT/TL module makes it possible to set the d-LED threshold level down to 2 mV. The best time resolution is obtained with the d-LED with an $\sim$4 mV threshold, and the resolution deteriorated as the threshold level increases. The measurement with the d-CFD method shows a similar tendency as in the d-LED: the best time resolution is obtained with a smaller fraction ($\sim$0.02), and the resolution becomes worse as the fraction value (shown in the upper axis) increases. In our previous study [7], we have measured the single photo-electron response of the MCP PMT/TL. The fact that these thresholds are smaller than the single photo-electron's amplitude suggests that the best timing resolution is decided by the first photo-electron arriving on the MCP PMT/TL. The simple d-LED method, with the use of a right threshold, is also observed to yield slightly better time pick-up than does the d-CFD method.

3.4. Position

For the measurement here, coincidence data taken using one MCP PMT/TL module and a R9800 PMT are used as in Section 3.2. Fig. 8(a) shows the energy spread profile observed in ten strip-lines from the events in [400,600] keV energy window. In the figure, the fraction of each strip-line energy is normalized by the energy sum of 10 strip-lines in each event, and the spread of the fraction is indicated by the error bar. The crystal position perpendicular to strip-line direction is calculated from 10 strip-line coordinates weighed by their energy. The measured position histogram for the 511 keV photo-peak events is shown in Fig. 8(b). Due to the fine 1.6 mm pitch between the strips, the position across the strips is determined precisely with a resolution of $\sim$0.3 mm (FWHM).

The position along the transmission-line is measured from the difference of pulse arrival time at both ends of the strip-line. To avoid the effect of gamma interaction spread along the crystal, a lead collimator with 1 mm diameter aperture is placed between the crystal and ^{22}Na source. Fig. 9(a) shows time difference ($\sim$41 ps FWHM) measured on the highest energy strip (#14 strip-line in Fig. 8(a)) from 511 keV photo-peak events.

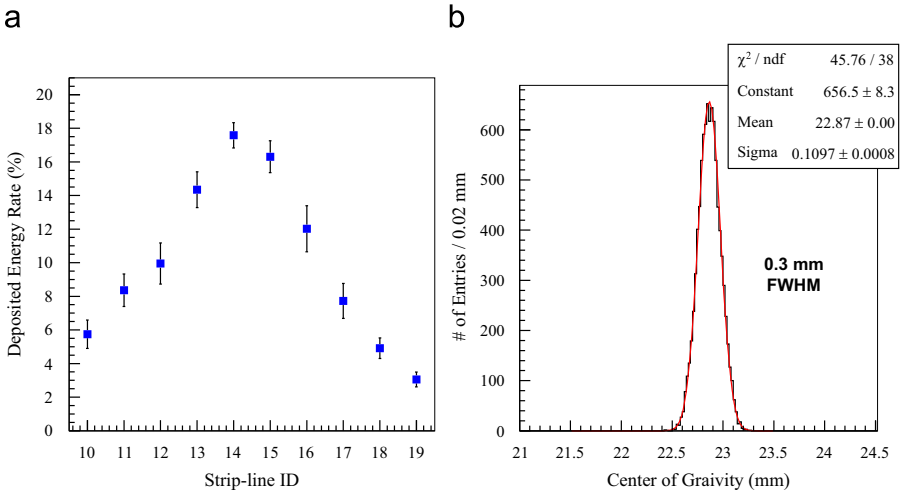

Fig. 8. (a) Energy profile measured in ten strip-lines from the 511 keV photo-peak events. (b) Crystal position perpendicular to the strip-line direction is calculated from the strip-line coordinates weighted with their energies; ~0.3 mm FWHM for the position resolution is measured.

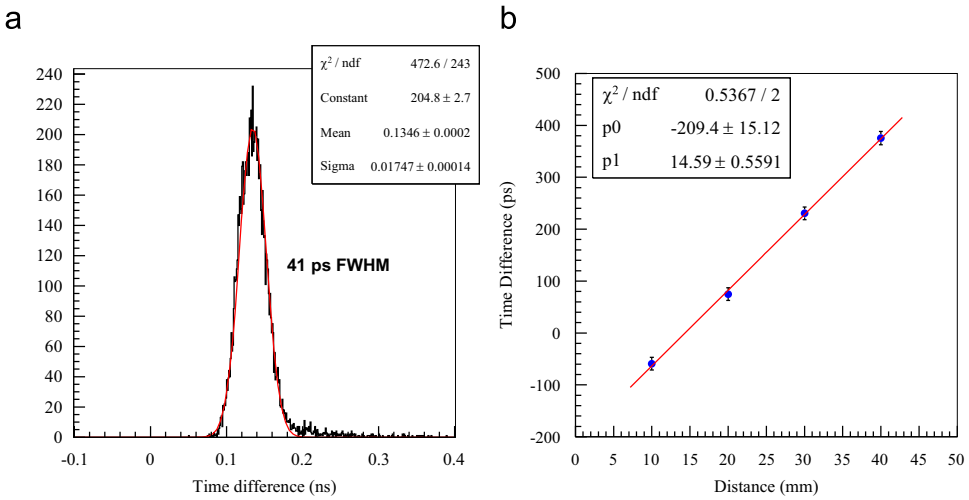

Fig. 9. (a) Arrival time difference of two signals at the two ends on the highest energy strip is measured from 511 keV photo-peak events. (b) The arrival time difference of two signals using a collimated LED is measured at different positions along a strip-line; the signal propagation speed on the strip-line is found to be 0.46*c*. The error bar in each point indicates the resolution of time difference, ~25 ps FWHM.

For conversion of the time difference to the path length, the signal propagation speed along the transmission-line is measured using a collimated light emitting diode (LED). The collimated light from a LED (CMD 204UWC-ND, MCL Tech. Inc.) through a 0.8 mm diameter aperture is sent to the MCP PMT window; the position of the LED on the MCP PMT is moved with a 10 mm step along a strip-line. The measured time difference on the strip-line at different positions is shown in Fig. 9(b). The resolutions of the time difference are measured to be ~25 ps FWHM, and are indicated by the error bars in the figure. The signal propagation speed is found to be 0.46*c* (*c* is a speed of light in vacuum), which is consistent with the estimated value using the TL printed circuit board (FR-4) parameters. From these two measurements, a ~2.8 mm position resolution along the strip-line is inferred from a ~41 ps FWHM in the time difference. A similar time resolution is obtained when rotating the crystal by 90°.

4. Discussion and summary

As a demonstration of large area flat panel MCP PMT based TOF PET, we have built PET detector modules using 2 in. × 2 in. Photonis XP85022 MCP PMTs. In the prototype module, transmission-line readout scheme is adopted to efficiently collect signals from the large area MCP PMT with smaller readout channels. For data acquisition, high speed waveform sampling by using the DRS4 evaluation boards is employed to maximize the fast time response of MCP PMT and also to precisely determine the event time. For the experimental tests, each MCP PMT/TL module is optically coupled to single LYSO crystal ($3 \times 3 \times 10$ mm^3) and responses to 511 keV annihilation photon are measured using the data taken in coincidence mode. Preliminary results obtained from a series of experiments can be summarized as follows: ~14% of energy resolution at 511 keV, ~309 ps (FWHM) coincidence time resolution, and position resolution of ~2.8 mm (0.3 mm) (FWHM) along (perpendicular to) the strip-line. This initial result gives a promise that the large area MCP PMT is applicable to TOF PET.

Acknowledgments

We are grateful for partial support of this work by the HEP Division of Argonne National Laboratory, a U.S. Department of Energy Office of Science laboratory, operated under Contract No.

DE-AC02-06CH11357, the NIH grant R21 CA131639-02, and a seed grant provided by the Women's Board of the University of Chicago.

References

[1] J.L. Wiza, Nuclear Instruments and Methods in Physics Research A 162 (1979) 587.
[2] K. Inami, N. Kishimoto, Y. Enari, M. Nagamine, T. Oshima, Nuclear Instruments and Methods in Physics Research A 560 (2006) 303.
[3] J. Va'vra, D.W.G.S. Leith, B. Ratcliff, E. Ramberg, M. Albrow, A. Ronzhin, C. Ertley, T. Natoli, E. May, K. Bryum, Nuclear Instruments and Methods in Physics Research A 606 (2009) 404.
[4] E. Morenzoni, K. Oba, E. Pedroni, D. Taqqu, Nuclear Instruments and Methods in Physics Research A 263 (1988) 397.
[5] A. Lehmann, et al., Nuclear Instruments and Methods in Physics Research A 595 (2008) 173.
[6] The Large-Area Picosecond Photo-detectors Project web page. ⟨http://psec.uchicago.edu/⟩.
[7] H. Kim, H. Frisch, C.-M. Kao, C.-T. Chen, J.-F. Genat, F. Tang, W.W. Moses, W.S. Choong, Nuclear Instruments and Methods in Physics Research A 622 (2010) 628.
[8] E. Delagnes, Y. Degerli, P. Goret, P. Nayman, F. Toussenel, P. Vincent, Nuclear Instruments and Methods in Physics Research A 567 (2006) 21.
[9] G. Varner, L. Ruckman, A. Wong, Nuclear Instruments and Methods in Physics Research A 591 (2008) 534.
[10] S. Ritt, R. Dinapoli, U. Hartmann, Nuclear Instruments and Methods in Physics Research A 623 (2010) 486.
[11] J.-F. Genat, G. Varner, F. Tang, H. Frisch, Nuclear Instruments and Methods in Physics Research A 607 (2009) 387.
[12] D. Breton, E. Delagnes, J. Maalmi, K. Nishimur, L. Ruckman, G. Varner, J. Va'vra, Nuclear Instruments and Methods in Physics Research A 629 (2011) 123.
[13] B. Joly, G. Montarou, J. Lecoq, G. Bohner, M. Crouau, M. Brossard, P. Vert, IEEE Transactions on Nuclear Science NS-57 (2010) 63.
[14] M. Aykac, I. Hong, S. Cho, Nuclear Instruments and Methods in Physics Research A 623 (2010) 1070.
[15] ⟨http://www.photonis.com⟩.
[16] J. Anderson, K. Byrum, G. Drake, C. Ertley, H. Frisch, J.-F. Genat, E. May, D. Salek, F. Tang, in: IEEE NSS/MIC Conference Record, 2008, pp. 2478–2481.
[17] DRS4 chip web page. ⟨http://drs.web.psi.ch/docs/DRS4_rev09.pdf⟩.
[18] C.W. Ueberhuber, Numerical Computation, Springer, Berlin, 1997.